

Detection of gravitational waves using topological data analysis and convolutional neural network: An improved approach

Christopher Bresten*

Department of AI and Data Science, Ajou University, Suwon 16499, Korea

Jae-Hun Jung†

Department of AI and Data Science, Ajou University, Suwon 16499, Korea

& Department of Mathematics, University at Buffalo,

State University of New York, Buffalo, NY 14260-2900, U.S.A.

(Dated: March 17, 2021)

The gravitational wave detection problem is challenging because the noise is typically overwhelming. Convolutional neural networks (CNNs) have been successfully applied, but require a large training set and the accuracy suffers significantly in the case of low SNR. We propose an improved method that employs a feature extraction step using persistent homology. The resulting method is more resilient to noise, more capable of detecting signals with varied signatures and requires less training. This is a powerful improvement as the detection problem can be computationally intense and is concerned with a relatively large class of wave signatures.

I. BACKGROUND AND MOTIVATION

The pioneering work by Huerta et al. [1] showed convolutional neural networks (CNN) to be a powerful method approach to the gravitational wave (GW) detection problem – a GW signature buried in the noisy interferometer data [2, 3] can be detected with a CNN. A CNN is a regularized multilayer artificial neural network that utilizes the hierarchical features in data [4, 5]. The localized nature of convolutions makes CNNs demonstrate great performance on raw data, especially image data. The approach is to train the CNN with noisy data with and without GW signatures. Data streams from interferometers are searched by matched-filter with a collection of approximate GW templates. When high correlation with a template is detected, it is shared with partners for verification with data sources from other interferometers and electromagnetic follow-up [3]. Appropriately trained CNNs have shown to be an excellent first pass detection method to proceed the more specific computationally expensive matched-filter and labor intense verification steps.

The original method of [1] followed the standard CNN architecture, so requires a large training set and a computationally cumbersome choice of hyper-parameters. Adding more feature selection prior to classification with CNN can improve performance.

In this letter, we propose a new method improving on the CNN approach by including topological features of the data, in particular, persistent homology of sliding window embeddings. This is known as topological data analysis (TDA) [6]. The proposed method makes training more efficient, consequently reducing the size of the training set significantly. The aforementioned localized effect

of convolution layers makes this a low-risk endeavor, as adding topological features should not decrease performance because as the CNN is trained, it can ignore these features by assigning small weights.

The important potential enhancement is the increased generality. Interesting GW signals come in a large and diverse class. For instance, multiple parameters are involved in a black-hole merger that change the signature, e.g. the mass ratio. TDA is a lossy process, but preserves various key properties such as period, decay rate, etc. when classifying wave-packets.

II. DATA SYNTHESIS

Signals were generated by a surrogate model described in [7]. The model generates non-spinning binary black-hole merger gravitational waveforms with mass ratio between 1 and 10. It has an accuracy close to that of the high-fidelity model which requires solving Einstein's equations by the *Spectral Einstein Code* (SpEC). The reduced model is constructed by selecting most relevant mass ratios using a greedy algorithm. The surrogate model is highly accurate after including about 15 waveforms, in that the error becomes comparable to the truncation error of the SpEC.

We use 1500 reference signals with mass ratios between 1.0078 and 9.9759, sampled at $2048Hz$. Each window length is 2 seconds. We construct training sets by adding noise and embedding the signal in noise so it occurs at a random time.

Let g be a signal from the reference set and ξ be the Gaussian noise with standard deviation 1. The GW signal g is embedded in ξ . The non-Gaussian noise can be treated in the similar manner. We scale the noise against the signal with a unitless scaling coefficient R . The synthetic data is then:

$$s = g + \epsilon \frac{1}{R} \xi. \quad (1)$$

* cbresten@ajou.ac.kr

† jaehunjung@ajou.ac.kr, jaehun@buffalo.edu

The coefficient $\epsilon = 10^{-19}$ scales the noise amplitude down to roughly the same order of magnitude as the signal. The signal is inserted at a random position in a piece of noise of duration 0.976 seconds (2000 elements at 2048Hz) scaled with the same factor as above. This yields a signal of length ≈ 2.976 seconds. A GW signal is present with probability of $p = 0.5$, implying that the training data is balanced. By cycling through a sample of signals and values for $0.075 < R < 0.65$ while randomly choosing signal presence and occurrence time, we construct an arbitrarily large training set. The coefficient R corresponds to the optimal match-filtered SNR in Table I.

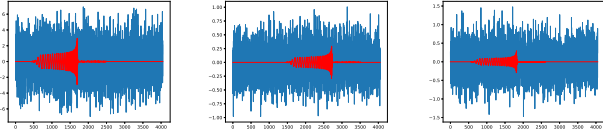


FIG. 1: Signals superimposed in red on noise with signal in blue. Random padding included. SNR: 12.519, 9.782, 6.874 left to right, respectively.

Figure 1 shows noisy signals (blue) that contain the GW (red) with SNR = 12.519, 9.782, 6.874, respectively. As shown in the figure, the GW is highly weak compared to the noise, so the detection is challenging.

Note that the noise is not Gaussian in general. It comes from various sources, terrestrial and astrophysical, giving color to the noise [8, 9]. Also note that SNR can be higher than the SNRs in the range used for our synthetic data [10, 11]. We focus on lower SNRs as we are interested in the limitations of the detection methods, though a SNR of below 10 is generally considered too low to be verifiable. Most detected signals have a SNR within the range we chose to test at the detection sites [3, 12–14].

III. SLIDING WINDOW EMBEDDING

We use the persistent homology of sliding window embeddings described in [15] (see Section IV for persistent homology). The main difference between the noise signal with and without the GW signal can be characterized by the periodic embedding of signals.

For a time-series f_k , $k \in \{1, \dots, N\}$ the sliding window embedding of size m at the time index j is:

$$(f_j, f_{j+1}, \dots, f_{m+j-1}), \quad (2)$$

where N is the number of samples and there are $N - m + 1$ points in \mathbb{R}^m . A periodic signal has a sliding window

TABLE I: Sample R and corresponding SNRs.

R	0.075	0.19	0.305	0.42	0.535	0.65
SNR	2.097	5.327	8.523	11.56	14.79	17.98

embedding of a circle or an oval. A decaying periodic signal is a spiral. White noise is a ball. They are easily classified using homology groups, providing a method to classify different periodic-like behaviors [15].

We chose $m = 200$, which is not optimized but chosen heuristically. Figure 2 shows the sliding window of white noise with SNR = 12.519, 9.782, 6.874.

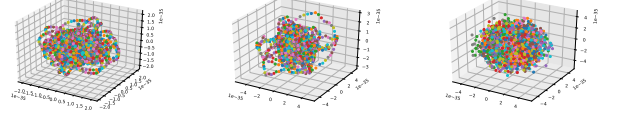


FIG. 2: Sliding window with noise, SNR descending left to right 12.519, 9.782, 6.874, respectively.

Dimensional reduction: The sliding window creates a point cloud in a m -dimensional space. However, the features of interest are much lower dimensional. We calculate feature persistent homology of H_1 , requiring 2 dimensions. This, along with the expense of TDA on high dimensional space, motivates a dimensional reduction before proceeding. We project down to three dimensions for ease of visualization and to avoid loss of using only two.

With the principal component analysis we project the data onto the first three singular vectors. Let M be a matrix containing each window of length $m = 200$ as a row. The point cloud is first centered at 0:

$$M_{:,j} = M_{:,j} - \overline{M_{:,j}}, \quad j \in \{0, 1, \dots, m-1\}, \quad (3)$$

where $M_{:,j}$ denotes the usual matrix element notation and $\overline{M_{:,j}}$ the mean value of j^{th} column vector of M . Then the singular value decomposition (SVD) is conducted and a projection operator is constructed to project the point cloud onto the first three scaled left singular vectors:

$$U\Sigma V^* = M, \quad (4)$$

$$\tilde{M} = M(\Sigma_{1:3,1:3} V_{1:3,:}^*)^*, \quad (5)$$

where $U\Sigma V^*$ is the SVD of M , \tilde{M} the reduction of M and the superscript $*$ the Hermitian conjugate.

Figure 3 is the dimensionally reduced sliding window embedding of a GW signal (left) and white noise (right). Notice that the topology of the white noise is approximately a ball, while the GW chirp signature has a different topology.

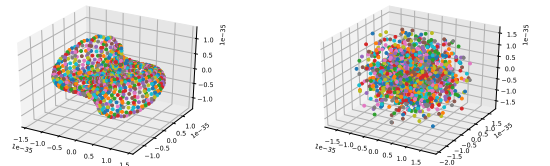


FIG. 3: Left: Sliding window of a GW signal with $m = 200$ after the dimensional reduction to 3. Right: Sliding window embedding of white-noise.

IV. TDA: PERSISTENT HOMOLOGY

Let X be the topological space of interest, the embedding space of GW signals in our case. Let σ_n be the n -simplex, the convex hull composed of $n+1$ vertices. Let \mathbf{R} be a ring and $C_n(X, \mathbf{R})$ be the free \mathbf{R} -module generated by all possible continuous images of n -simplices σ_n . Let $\delta_n: C_n \rightarrow C_{n-1}$ be the boundary map as

$$\delta_n \sigma_n = \sum_{k=0}^n (-1)^k [p_0, \dots, p_{k-1}, p_{k+1}, \dots, p_n]$$

where $\{p_i\}$ are the vertices. The factor $(-1)^k$ is put to preserve the orientation. The n th homology group of X with coefficients in \mathbf{R} , $H_n(X, \mathbf{R})$, is the quotient group of the kernel and image groups:

$$H_n(X, \mathbf{R}) = \ker(\delta_n) / \text{im}(\delta_{n+1}).$$

The number of generators of $H_n(X, \mathbf{R})$ is called the Betti number, β_n , roughly the number of geometric holes in n th dimensional space of X . β_0 denotes the number of connected components. For example, for S^2 , $H_0 = 1$, $H_1 = 0$ and $H_2 = 1$ and for T^2 , $H_0 = 1$, $H_1 = 2$ and $H_2 = 1$.

Given the point cloud, we construct a simplicial complex created by gluing a finite number of simplices together. Homology on such a simplicial complex is known as persistent homology. We use the Vietoris-Rips complex [6], which is built by taking all points as zero simplices. For a fixed value of t , known as the filtration parameter, we add edges between two points if their distance is less than t . We add a triangle between three points if each pair of points has distance less than t and so on for higher dimensional simplices. We repeat this process with various t values.

The barcode is the graph of β_n against the parameter t . It displays not only β_n at each t , but also graphs how long each generator remains non-trivial. Its interval gives a concept referred to as *persistence*. The starting point of each persistence is called “birth” and the ending “death”. Its vertical representation, with the birth as x -axis and the death y -axis, is called the persistence diagram.

Let l_0 be the number of the persistences in H_0 barcode and l_1 in H_1 . Once both barcodes are obtained, we sort the persistences by descending magnitude. Let π_i^0 be the ordered persistence in H_0 , $i = 1, 2, \dots, l_0$, similarly π_i^1 the ordered persistence in H_1 , $i = 1, 2, \dots, l_1$. Let Π^0 and Π^1 be

$$\begin{aligned} \Pi^0 &= (\pi_1^0, \pi_2^0, \dots, \pi_{l_0}^0), \\ \Pi^1 &= (\pi_1^1, \pi_2^1, \dots, \pi_{l_1}^1). \end{aligned}$$

We call these persistence vectors, and they are how we choose to encode topological features as a vector that can be used as input to a CNN.

We use the persistent homology for dimensions 0 and 1 because the existing results regarding TDA of sliding

window embeddings focus on H_1 [15]. H_0 was included as the performance impact of doing so was negligible and the nature of a CNN allows for it to be used or disregarded as fit. The Vietoris-Rips complex is computationally feasible as we use only H_0 and H_1 but may become extremely resource intense for higher order homology groups.

V. PREPROCESSING FOR CNN

The persistence vectors Π^0, Π^1 (of length l_0, l_1 respectively) are adjusted to a fixed length N_p by either truncation or zero-padding as needed. These are then concatenated into one vector Π , of length $2N_p$:

$$\Pi = (\Pi^0, \Pi^1). \quad (6)$$

The raw signal is then concatenated with Π :

$$\mathbf{x} = (\text{signal}, \Pi). \quad (7)$$

The resulting vector \mathbf{x} is of fixed size and ready for input into the CNN. In the actual procedure, we first normalize Π and *signal* separately so that they have the same maximum. A similar approach has been applied to VLBI signal analysis [16].

VI. HYPER-PARAMETERS & PROCEDURE

The hyper-parameters used here are meant to replicate the work in [1]. They are suboptimal but we use them for comparison purpose. We used mean-squared error for the loss function and Adam optimizer [17] for optimization. Five epochs were used for training. The size of the synthetic data sets is 30,000. This was divided into 20,000

TABLE II: The hyperparameters are used to replicate the work in [1].

Number	Type	Parameters
1	Input	
2	Convolution	64, strides = 1, kernel size = 16
3	Max Pooling	strides = 4, pool size = 4
4	Dense	64, ReLU
5	Convolution	128, strides = 1, kernel size = 16
6	Max Pooling	strides = 4, pool size = 4
7	Dense	128, ReLU
8	Convolution	256, strides = 1, kernel size = 16
9	Max Pooling	strides = 4, pool size = 4
10	Dense	256, ReLU
11	Convolution	512, strides = 1, kernel size = 32
12	Max Pooling	strides = 4, pool size = 4
13	Dense	512, ReLU
14	Flatten	
15	Dense	128, Linear
16	Dense	128, ReLU
17	Dense	64, Linear
18	Dense	64, ReLU
19	Dense	2, Linear

elements for training and 10,000 for testing. Initialization function was `Orthogonal()` in Keras. Random seeds were fixed everywhere necessary to force deterministic initialization and optimization for reproducibility. The procedure is as follows:

1. Generate sliding window embedding (SWE) of the raw signal
2. Perform the dimensional reduction on the SWE, yielding a 3-dimensional point cloud
3. Compute persistent homology of H_0 and H_1 of the SWE
4. Construct Π with a fixed N_p
5. Normalize Π and raw data
6. Concatenate Π and the raw signal
7. Input into CNN for binary classification

VII. RESULTS

Performance metrics: *Sensitivity* is the ratio of true positives to all positives and *specificity* is the ratio of true negatives to all negatives. They are also called the true positive rate (TPR) and true negative rate (TNR), respectively. A perfect classifier has both equal to 1. The case of 0.5 is equivalent to using a coin toss as a binary classifier. The case where $\text{TPR} = 1$ and $\text{TNR} = 0$ corresponds to a case where the classifier always guesses positive regardless of input, vice versa if the classifier always guesses negative.

The receiver operating characteristic (ROC) curves are another metric for the evaluation. The closer the area under the curve (AUC) to 1, the better the classifier. A perfect binary classifier is a step function that reaches 1 at $x = 0$. A classifier of $y = x$ shows no classification ability equivalent to a coin fair flip.

Software: We used GUDHI [18, 19] for TDA and Keras for CNN as an interface to Tensorflow. For the ROC curves `sklearn.metrics.roc_curve()` was used. For the sensitivity and specificity vs SNR curves, our own routine was used with a fixed threshold value of 0.5. `python-gwtools` was used to calculate the optimal match-filtered SNR [20].

Figures 4, 5, 6 and 7 show two performance metrics for three different training and test sets. The blue solid line represents the CNN with raw data, the red the CNN with TDA features only (Eq. (6)) and the green the CNN with raw data and TDA features concatenated (Eq. (7)), labeled as *raw*, *tda*, *both*. Each contains 20,000 training elements, 50% of which have a GW signal. The test set has 10,000 elements synthesized in the same manner as the training set. The first set uses 11 different signals of different mass ratios, as well as 10 different SNRs. The other two sets use only one signal with 30 uniform samplings and 100 SNRs respectively, for $R \in [0.075, 0.65]$. The left shows the sensitivity and specificity for each method versus SNR.

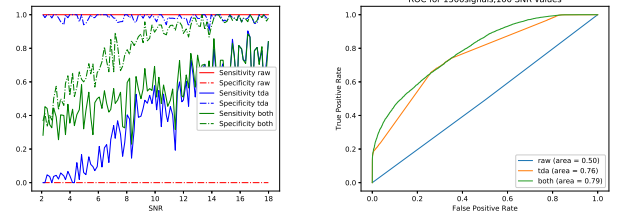


FIG. 4: Hardest case, 1500 different GW signals of mass ratio 1 to 9.97 sampled at 100 different SNRs. Raw signal has no detection capability

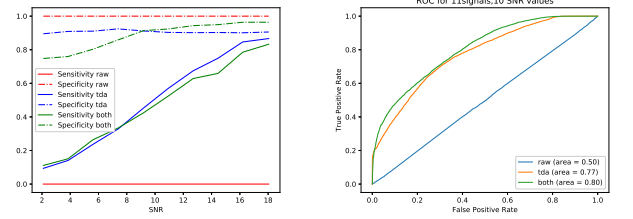


FIG. 5: Hard case, 11 different GW signals of mass ratio 1 to 9.97 sampled at 10 different SNRs. Raw signal has no detection capability

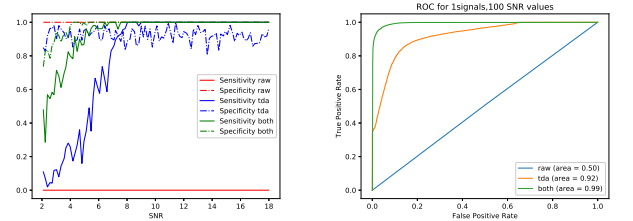


FIG. 6: 100 different SNRs. Raw signal alone has no detection capability.

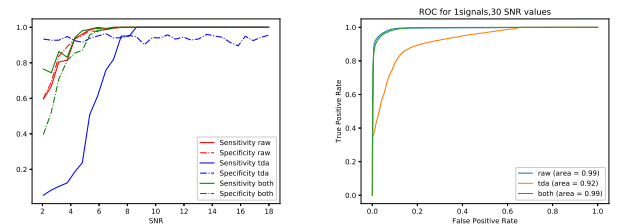


FIG. 7: Easiest case, only 30 different SNRs, 1 signal.

As detection is more difficult when there are a wider range of signals and SNR values (Fig. 4 and Fig. 5), these tests are descending in difficulty, Fig. 7 being the easiest case and Fig. 4 being the hardest. It is clear that using the CNN with the raw signal alone provides no detection ability except for the easiest case (Fig. 7), while the TDA features alone provide some detection ability in all cases, and the combined features are better in every case. This shows the power of the topological features to greatly

improve performance, and the synergy of combining them with the raw signal (which increases maximum accuracy).

Figures 8, 9, 10 have a constant SNR and use 1500 signals with mass ratios between 1.0078 and 9.9759. The training set sizes are 11000, 4000, 1500 and test set sizes 4000, 2000, 1500, respectively. They show the effect of noise level and training set size on the efficacy of the method. They show that the TDA features are responsible for increased accuracy at lower SNR with less training. Note that when training the CNN with TDA features alone, performance does not change much as the training set size increases. It is worth noting that when using TDA features alone, performance maximizes after a relatively small training set. This lends to the assertion that the TDA features reduce the training requirements of the scheme.

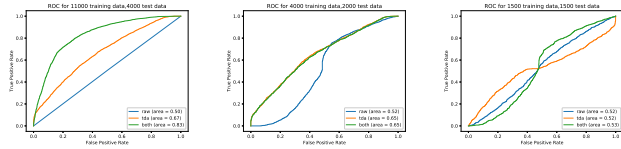


FIG. 8: SNR of 6.874.

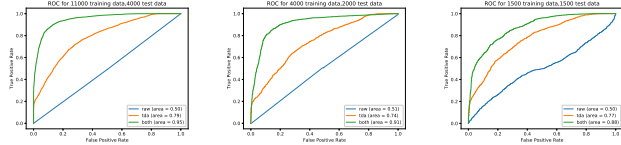


FIG. 9: SNR of 9.782.

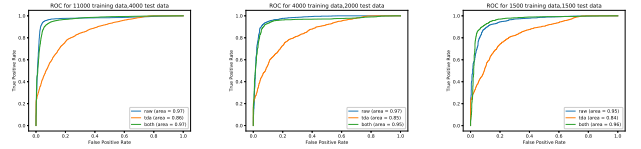


FIG. 10: SNR of 12.519.

As these examples indicate, the proposed method yields a significant improvement over the original CNN method. It could be very useful for pre-screening the interferometer data-streams to locate potentially interesting windows before more costly analysis. It is not limited to the detection of black-hole mergers, as many interesting astrophysical sources of gravitational wave produce a chirp type of signature [21].

ACKNOWLEDGMENTS

The authors thank Scott Field for providing data and for the helpful discussion. This work was supported by National Research Foundation.

- [1] D. George and E. Huerta, *Physics Letters B* **778**, 64 (2018).
- [2] B. P. Abbott, R. Abbott, T. Abbott, M. Abernathy, F. Acernese, K. Ackley, C. Adams, T. Adams, P. Addesso, R. Adhikari, *et al.*, *Physical review letters* **116**, 061102 (2016).
- [3] B. P. Abbott, R. Abbott, T. D. Abbott, F. Acernese, K. Ackley, C. Adams, T. Adams, P. Addesso, R. X. Adhikari, V. B. Adya, C. Affeldt, *et al.* (LIGO Scientific Collaboration and Virgo Collaboration), *Phys. Rev. Lett.* **119**, 141101 (2017).
- [4] Y. LeCun, B. E. Boser, J. S. Denker, D. Henderson, R. E. Howard, W. E. Hubbard, and L. D. Jackel, in *Advances in neural information processing systems* (1990) pp. 396–404.
- [5] Y. LeCun, B. Boser, J. S. Denker, D. Henderson, R. E. Howard, W. Hubbard, and L. D. Jackel, *Neural computation* **1**, 541 (1989).
- [6] G. Carlsson, *Bulletin of the American Mathematical Society* **46**, 255 (2009).
- [7] J. Blackman, S. E. Field, C. R. Galley, B. Szilágyi, M. A. Scheel, M. Tiglio, and D. A. Hemberger, *Physical review letters* **115**, 121102 (2015).
- [8] B. P. Abbott, R. Abbott, T. Abbott, M. Abernathy, F. Acernese, K. Ackley, M. Adamo, C. Adams, T. Adams, P. Addesso, *et al.*, *Classical and Quantum Gravity* **33**, 134001 (2016).
- [9] B. Allen, J. D. Creighton, É. É. Flanagan, and J. D. Romano, *Physical Review D* **65**, 122002 (2002).
- [10] B. P. Abbott, R. Abbott, T. Abbott, M. Abernathy, F. Acernese, K. Ackley, C. Adams, T. Adams, P. Addesso, R. Adhikari, *et al.*, *Physical review letters* **116**, 061102 (2016).
- [11] B. P. Abbott, R. Abbott, T. Abbott, F. Acernese, K. Ackley, C. Adams, T. Adams, P. Addesso, R. Adhikari, V. Adya, *et al.*, *Physical Review Letters* **119**, 161101 (2017).
- [12] B. P. Abbott, R. Abbott, T. Abbott, M. Abernathy, F. Acernese, K. Ackley, C. Adams, T. Adams, P. Addesso, R. Adhikari, *et al.*, *Physical review letters* **116**, 241103 (2016).
- [13] L. Scientific, B. Abbott, R. Abbott, T. Abbott, F. Acernese, K. Ackley, C. Adams, T. Adams, P. Addesso, R. Adhikari, *et al.*, *Physical Review Letters* **118**, 221101 (2017).

- [14] B. P. Abbott, R. Abbott, T. Abbott, F. Acernese, K. Ackley, C. Adams, T. Adams, P. Addesso, R. Adhikari, V. Adya, *et al.*, The Astrophysical Journal Letters **851**, L35 (2017).
- [15] J. A. Perea and J. Harer, Foundations of Computational Mathematics **15**, 799 (2015).
- [16] D. Lee, C. Bresten, K. Youm, K.-W. Seo, and J.-H. Jung, Submitted (2019).
- [17] D. P. Kingma and J. Ba, arXiv preprint arXiv:1412.6980 (2014).
- [18] C. Maria, J.-D. Boissonnat, M. Glisse, and M. Yvinec, in *International Congress on Mathematical Software* (Springer, 2014) pp. 167–174.
- [19] “Gudhi :: Anaconda cloud,” <https://anaconda.org/conda-forge/gudhi> (2018), accessed: 2018-10-20.
- [20] “gwtools 1.0.2: A collection of gravitational wave tools,” <https://pypi.org/project/gwtools/> (2019), accessed: 2019-07-15.
- [21] B. P. Abbott, R. Abbott, T. Abbott, F. Acernese, K. Ackley, C. Adams, T. Adams, P. Addesso, R. Adhikari, V. Adya, *et al.*, Physical Review Letters **119**, 161101 (2017).